Published in Hydrological Sciences Journal 55, issue 8, 1325-1336, 2010
which should be used for any reference to this work

Grid-enabled Monte Carlo analysis of the impacts of uncertain discharge rates on seawater intrusion in the Korba aquifer (Tunisia)

Jaouher Kerrou[1], Philippe Renard[1], Giuditta Lecca[2] & Jamila Tarhouni[3]

[1]*Centre for Hydrogeology, University of Neuchâtel, Rue Emile Argand 11, CP158, CH-2009 Neuchâtel, Switzerland*
jaouher.kerrou@unine.ch

[2]*Centre for Advanced Studies, Research and Development in Sardinia, CRS4, Edificio 1, Parco Tecnologico "Sardegna Ricerche", I-09010 Pula (Cagliari), Italy*

[3]*Institut National Agronomique de Tunisie, Avenue Charles Nicolle 43, 1082 Tunis-Mahrajène, Tunisia*

Abstract The Korba aquifer, located in the north of Tunisia, suffers heavily from salinization due to seawater intrusion. In 2000, the aquifer was exploited from more than 9000 wells. The problem is that no precise information was recorded concerning the current extraction rates, their spatial distribution, or their evolution in time. In this study, a geostatistical model of the exploitation rates was constructed based on a multi-linear regression model combining incomplete direct data and exhaustive secondary information. The impacts of the uncertainty on the spatial distribution of the pumping rates on seawater intrusion were evaluated using a 3-D density-dependent groundwater model. To circumvent the large amount of computing time required to run transient models, the simulations were run in a parallel fashion on the Grid infrastructure provided by the Enabling Grid for E-Science in Europe project. Monte Carlo simulations results showed that 8.3% of the aquifer area is affected by input uncertainty.

Key words seawater intrusion; numerical modelling; geostatistics; uncertainty; grid computing

Utilisation d'une grille de calcul pour une analyse de Monte Carlo des impacts de l'incertitude liée aux débits d'exploitation sur l'intrusion marine dans l'aquifère de Korba (Tunisie)
Résumé L'aquifère de Korba, situé au nord de la Tunisie, est gravement touché par une salinisation du à l'intrusion marine. En 2000, l'aquifère a été exploité par plus de 9000 puits. Le problème, c'est qu'il n'y a pas d'information précise concernant les débits de pompage, leur répartition dans l'espace ainsi que leur évolution dans le temps. Dans cette étude, un modèle géostatistique des débits d'exploitation a été construit en se basant sur une régression multilinéaire combinant des données directes incomplètes ainsi que des données secondaires exhaustives. Les impacts de l'incertitude associée à la distribution spatiale des débits de pompage sur l'intrusion marine ont été évalués en utilisant un modèle tridimensionnel d'écoulement et de transport à densité variable. Pour contourner les difficultés liées à de longs temps de calcul, nécessaires pour résoudre des problèmes en régime transitoire, les simulations ont été réalisées en parallèle sur une grille informatique de calcul mise à disposition par le projet "Enabling Grid for E-Science in Europe". Les résultats des simulations de Monte Carlo ont montré que 8.3% de la surface de l'aquifère est affectée par l'incertitude liée aux données d'entrée.

Mots clefs intrusion marine; modélisation numérique; géostatistique; incertitude; grille de calcul

1 INTRODUCTION

In 2001, over half the world's population was living within 200 km of the coast and represented as many people as the entire population in 1950 (United Nations Foundation, 2008). Such a demographic growth in coastal areas has greatly increased freshwater demand, especially for agricultural purposes. Groundwater resources in these areas are therefore intensively exploited despite their extreme vulnerability to seawater intrusion. To provide recommendations to managers, it is important to understand the dynamics of coastal aquifers and to be able to model them. Nowadays, many codes allow seawater intrusion to be modelled as coupled density-dependent groundwater flow and miscible solute transport (Sorek & Pinder, 1999). The validity and usefulness of using these numerical models

has been demonstrated extensively in numerous research and case studies (Bear *et al*., 1999; Diersch & Kolditz, 2002; Cheng & Ouazar, 2003; Milnes & Renard, 2004).

Nevertheless, these models are affected by different sources of uncertainty (Carrera, 1993). One of the most significant is the effect of uncertainty due to the heterogeneity of the hydraulic conductivity. This problem has been investigated numerically and analytically under different assumptions (Dagan & Zeitoun, 1998; Naji *et al*., 1998; Al-Bitar & Ababou, 2005; Abarca, 2006). In addition, it is frequent that extraction rates are also highly uncertain. Not having detailed information about extraction rates is a problem encountered in many countries worldwide (Custodio, 2002; Konikow & Kendy, 2005).

In the Korba aquifer (Tunisia), the local water management authority identified more than 9000 active wells in a region covering around 400 km^2. Most of the wells located in very small farms are traditionally dug, shallow, and equipped with oil motor pumps. None of these wells is equipped with a flow meter and no survey has ever been made to estimate exhaustively their exploitation rates.

Kerrou *et al*. (2010) built a multi-linear regression model to estimate the pumping rates in the Korba aquifer by combining a series of explanatory exhaustive variables describing the state of the aquifer, its properties, as well as data from remote sensing analysis. The pumping rate estimates were then used to calibrate a three-dimensional (3-D) density-dependent flow and miscible solute transport model, but without accounting for the uncertainty in the estimated pumping rates, in particular their spatial distribution. Therefore, the main aim of the present work is to study how this uncertainty can be modelled and to investigate its impact on seawater intrusion. This work focuses only on uncertainty in the pumping rates, while other sources of uncertainty are possible (e.g. hydraulic conductivity, effective recharge, etc.). The approach adopted here is to set up a geostatistical model of the pumping rates based on the regression model (Kerrou *et al*., 2010), in order to generate a large number of equally likely simulations. The next step consists of propagating this uncertainty into a realistic 3-D density-dependent groundwater model by running Monte Carlo simulations.

However, running such complex and regional seawater intrusion models on a single PC for a sufficient number of stochastic realizations is often just not feasible. That difficulty can be overcome by using a cluster of computers on which each stochastic realization is executed independently. This is a common technology today, but it still remains rather expensive and not all laboratories have access to such an infrastructure, particularly where hydrogeologists are located in countries with low incomes. This is an issue because these countries also frequently face the problem of seawater intrusion and uncertainty with the most dramatic consequences for their economy. Therefore, the second aim of the paper is to investigate whether the Grid computing infrastructure provided by the Enabling Grid for E-Science in Europe project could be used to run the Monte Carlo simulations remotely, and possibly directly, from the countries where the problems occur. Grid computing (Foster & Kesselman, 1998) is an emerging technology that allows users to launch computations on a distributed network of computing resources without having to deal with the process of remote log-in, transferring the data back and forth, launching the jobs, etc. All these aspects are handled by "middleware" which is software that allows the user to connect securely to the Grid and run the jobs. The Grid takes care of finding a machine that is available, transfers the information, runs the job, and sends the results back. While that vision is very appealing and extremely well adapted for running Monte Carlo simulations, there are nowadays only a limited number of Grid infrastructures that are running at a large scale. Furthermore, the technology is still in development and not always stable and this is why it is interesting to study whether the exercise can be done or not.

In summary, the aims of this study are: (a) to investigate how to model and propagate the uncertainty on the spatial distribution of the extraction rates to seawater intrusion model outputs, especially head and salt concentration distributions; and (b) to test whether it is feasible to use Grid technology to run Monte Carlo simulations. These two questions are addressed by treating the example of the Korba aquifer.

2 SITE DESCRIPTION

The Korba aquifer is located in the Cape Bon peninsula in Tunisia (Fig. 1). It covers approximately 400 km^2 and has been extensively studied (Ennabli, 1980; Tarhouni *et al*., 1996; Khlaifi, 1998; Paniconi *et al*., 2001; Slama *et al*., 2008; Kouzana *et al*., 2009; Kerrou *et al*., 2010).

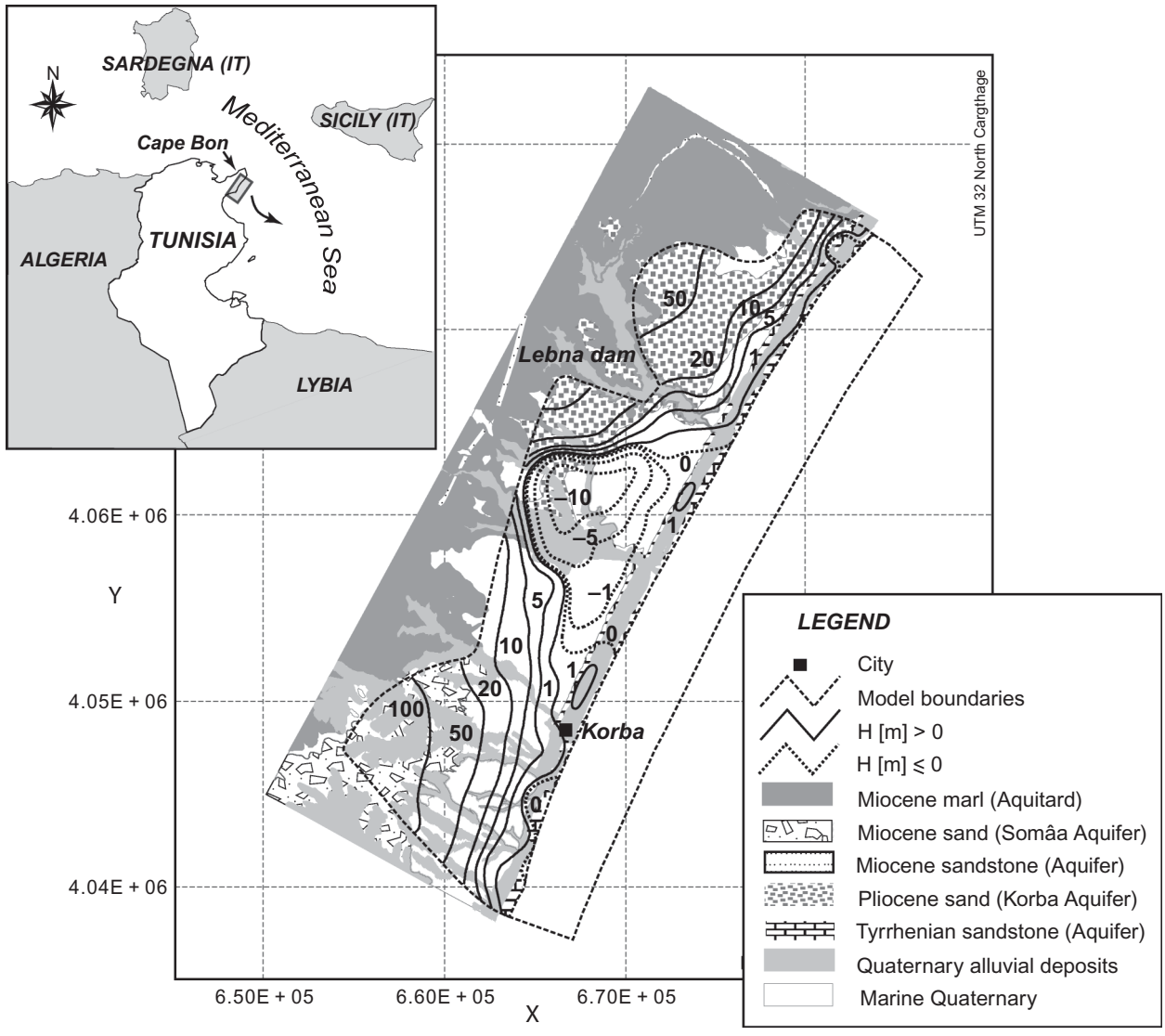

Fig. 1 Location map of the Korba aquifer and geological settings (squares are 10 × 10 km). Hydraulic heads observed in August 2004 are also shown.

Three main geological formations constitute the aquifer system. The first is of Tyrrhenian (Quaternary) age forming an approx. 1.2-km-wide band parallel to the coast all along the domain. It is constituted mainly by arenitic limestone underlain by a conglomeratic layer (Oueslati, 1994) and its thickness varies between 10 and 50 m. The second formation is of Pliocene age and corresponds to marine sediments deposited in the Dakhla syncline in the north of the city of Korba. The dominant lithologies in that formation are yellow sands with alternating clay and sandstone levels. The third formation, called "the sands of Somâa", is of late Miocene age and is located only in the south of the study area. It is composed mainly of thick fine sand layers of continental origin including conglomeratic levels and clay lenses. The thickness of the Pliocene formation might reach 250 m offshore, decreasing toward the west, while the thickness of the Somâa formation exceeds 400 m (Kerrou *et al*., 2010). The aquifer layers are underlain by Miocene marls forming the bedrock of the system (Ennabli, 1980). This aquitard contains lenticular sandstone bars of variable thickness and depth, often separated by thick layers of almost impervious marls.

The aquifer is essentially unconfined. The Plio-Quaternary units, which constitute the largest part of the aquifer (north of Somâa), are the most productive and are characterized by the highest transmissivity.

Kerrou *et al*. (2010) estimated the hydraulic conductivity of the Quaternary arenitic limestone to be around 10^{-4} m/s, that of the Pliocene formation 5×10^{-5} m/s and that of the Somâa 6×10^{-6} m/s. The same authors estimated the natural recharge of the aquifer by infiltration of precipitation to be around 29 hm^3/year, with high variability in space and time, and ranging between 8 and 30% of the mean annual rainfall of 420 mm/year. However, the abstraction rates which started in the early 1960s (Ennabli, 1980), mainly for irrigation purposes, were estimated to range around 50 hm^3/year from the early 1980s to 2004 (Kerrou *et al*., 2010).

Under natural conditions, groundwater flows towards the sea. However, due to the intense groundwater abstraction, hydraulic gradients have been reversed mainly toward the central part of the aquifer, leading to enhanced seawater intrusion. In 2004, the piezometric map showed a wide depression in the central part of the aquifer (Fig. 1) where the hydraulic head went down to 12 m below the mean sea level. Vertical salinity profiles in the wells at 2 km from the shoreline showed total dissolved solids (TDS) values ranging between 2 and 15 g/L, confirming the landward seawater encroachment. Kerrou *et al*. (2010) estimated that the seawater intrusion velocity was of the order of 100 m/year during the last decade, corresponding to around 7 hm^3/year of saltwater entering the aquifer.

3 METHODOLOGY

3.1 Geostatistical model of the pumping rates

The geostatistical model of the pumping rates developed for the purposes of the present study is based on the multi-linear regression model built by Kerrou *et al.* (2010). For a better understanding of the approach adopted herein, the previous statistical framework is presented briefly. Kerrou *et al.* (2010) used a set of 432 measured pumping rates (Fig. 2(a)) as a reference to construct a multi-linear regression model. The latter combines eight secondary parameter distributions: aquifer transmissivity; crop evapotranspiration; electrical conductivity; seasonal head variation; water-table depth; historical piezometric decline; distance to the sea; and digital elevation model. The pair-wise correlations between these parameters and measured pumping rates were analysed and showed statistically significant correlations (e.g. pumping rates with transmissivity and with crop evapotranspiration), and others relatively weak correlations (e.g. pumping rates with distance to the sea and with elevation). Then, a multi-linear model was estimated by standard linear least squares and used to estimate the pumping rates over the whole aquifer using the eight exhaustively mapped variables (Fig. 2 (a)). The multi-linear regression model fit is not very accurate and an important residual error is clearly visible on the plot of estimated *versus* measured discharge rates (Fig. 2(b)).

In this study, the statistics and the spatial distribution of the residuals, *e*, between the measured pumping rates and those computed by the multi-linear regression model were analysed in a geostatistical framework. It was found that the residuals could be approximated by a Gaussian distribution (Fig. 2(c)) of zero mean and 21×10^3 m^3/year standard deviation. The experimental variogram (Fig. 2(d)) showed a spatial structure, indicating that the errors correlate over distances of up to 700 m. The experimental variogram was then modelled using an exponential model with a range of 700 m (Fig. 2(d)). In order to allow more spatial continuity of the pumping rates at small scales, it was decided not to use a nugget effect in the model.

Based on the variogram model and the Gaussian distribution, unconditional simulations using the turning band method (Matheron, 1973; Tompson *et al*., 1989) were performed to generate 100 residual (*e*) maps over the whole domain. The grid used to simulate the residuals is the same as that used in Kerrou *et al*. (2010) to estimate the average pumping rates map and corresponds to the well density 300×300 m resolution grid. Each residual map was added to the average one (estimated by the multi-linear regression) to obtain 100 equally likely realizations of maps of pumping rates all sharing the same total volume. Then, two typical time-dependent functions were used to distribute pumping rates in time in all the wells.

3.2 The Korba aquifer 3-D numerical model

The numerical groundwater model used to propagate the uncertainty on the pumping rates for seawater intrusion forecasts was developed in Kerrou *et al.* (2010) and built with GroundWater simulator (Cornaton, 2007). GroundWater is a three-dimensional simulator. It solves a broad range of coupled processes, including variably saturated flow, density-dependent flow, heat and thermo-haline transport, as well as groundwater age. The flow equations are solved using a finite-element Galerkin technique. For the Korba aquifer, a confined 3-D density-dependent model was used in order to allow a better reproduction of hydraulic head

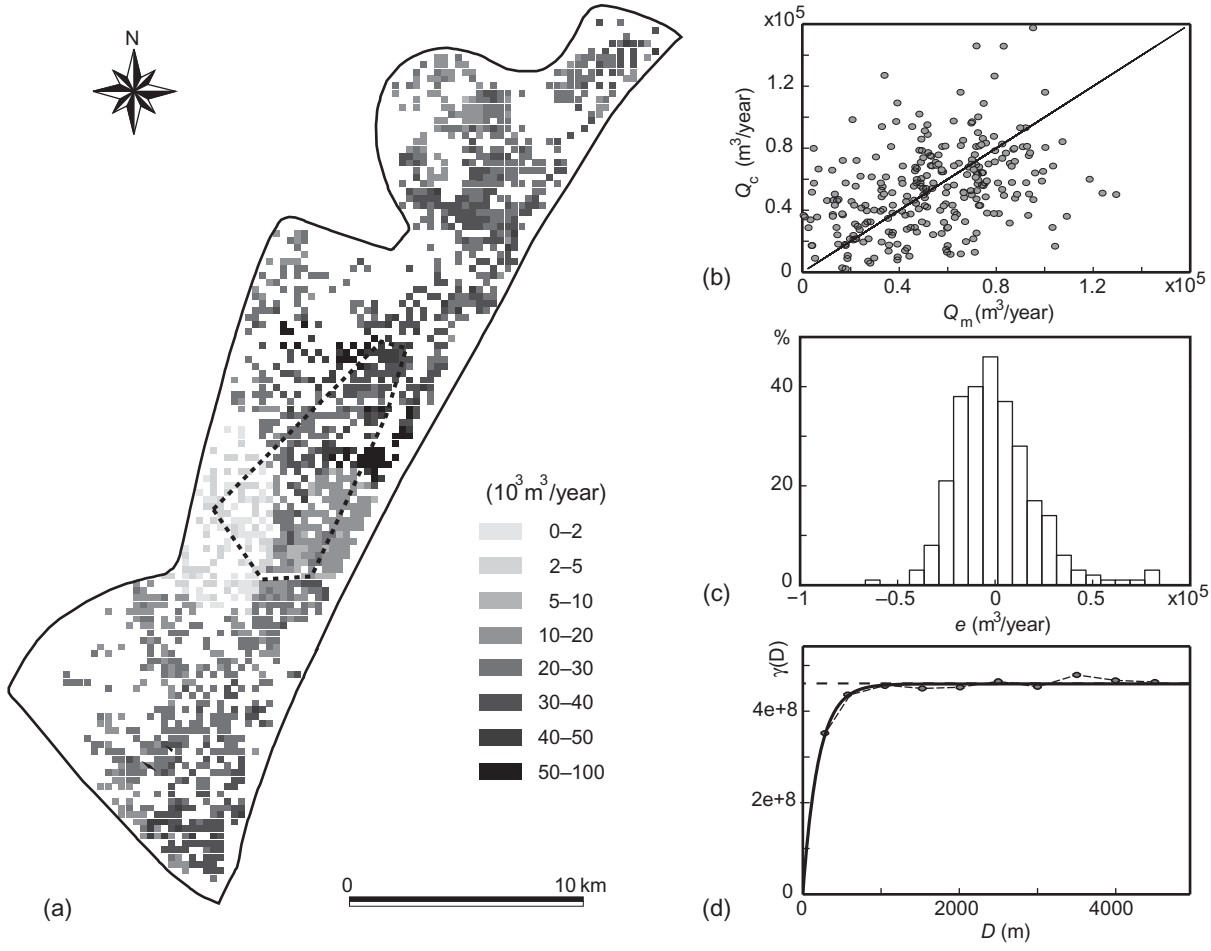

Fig. 2 (a) Average pumping rates map after Kerrou *et al*. (2010) with the location of the exhaustive pumping rate survey (dashed line polygon). (b) Scatter plot of estimated Q_c *versus* measured Q_m pumping rates; (c) histogram of the residual e; and (d) experimental (o) and model (——) variograms of the error.

and salt concentration vertical gradients, and to account for lateral and especially vertical changes in the hydrodynamic parameters of the aquifer (e.g. Pliocene and Miocene units). The mesh honouring the 3-D geometry of the aquifer was discretized into 877 249 prismatic finite elements and 19 layers (Fig. 3), with local refinement in the main aquifer (Pliocene) and close to the sea.

The steady-state flow boundary conditions are a prescribed head on the seafloor and constant lateral inflow on the northern part of the Pliocene. The seaside boundary extends 3.5 km offshore (arbitrary fixed) to avoid unrealistic boundary effects. In transient regime, additional lateral fluxes were attributed to account for recharge from the Lebna Dam and additional well type boundary conditions with increasing discharge rates. The map of the ranges of possible recharge of the aquifer by infiltration of precipitation (on the top layer) was estimated from 1960 to 2004, by the daily Thornthwaite-Mather method (Steenhuis & Vandermolen, 1986), using the regional soil distribution (100 × 100 m grid) with relative field capacities, daily rainfall and pan evaporation data. These ranges of aquifer recharge were then used to constrain the calibration of the final recharge map with the numerical model (Kerrou *et al.*, 2010). It is worth noting that 1498 time-dependent functions (1491 for the well clusters, six for the areal recharge and one for the lateral recharge) were implemented in the model.

With regard to transport boundary conditions, a maximum relative seawater concentration of 1 [-] was assigned at the seafloor only to inward seawater fluxes (water enters the aquifer with seawater concentration but exits with the aquifer concentration).

The calibration of the 3-D model against field observations was achieved in a time-dependent, iterative, constrained and semi-automatic fashion using the PEST

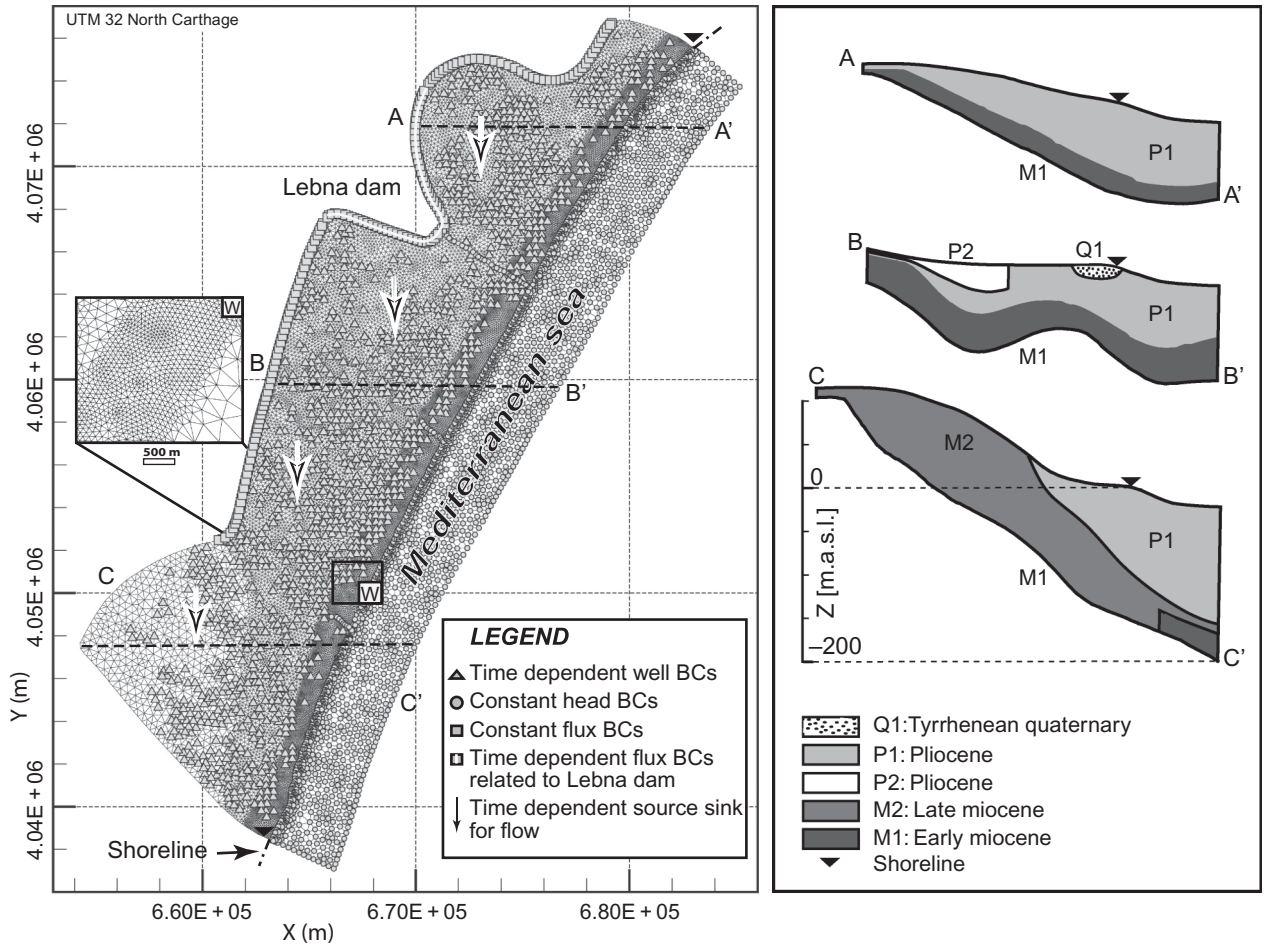

Fig. 3 The Korba aquifer 3-D numerical model, modified after Kerrou *et al*. (2010). Note that wells were attributed at around 10 m from model surface and the lateral fluxes were integrated over the Pliocene formation thickness. Element sizes range from 150 to 200 m in the main aquifer and between 50 and 100 m near the shoreline. Vertically, the mesh is divided into 19 layers with 5 m thickness on average.

software (Doherty, 1998) for flow, and by trial and error for transport. First, a steady-state flow model was calibrated to estimate hydraulic conductivity and recharge, and then a 44-year transient regime flow model with steady-state solutions as initial conditions was calibrated to estimate storativity. A total of 1753 time-dependent measured heads and 881 measured concentrations were used as control data. The model was calibrated to reproduce the long-term depletion of groundwater levels. Constant values for dispersivity and porosity were calibrated by trial and error in order to reproduce the seawater encroachment in the Korba aquifer. The dispersivity values were chosen sufficiently large to avoid competition with numerical dispersion in the largest elements. As a result, a root mean square error (RMSE) of 6.2 m for heads ($-12 < H_{obs} < 120$ m) and 6.69 g/L for salt concentrations ($0.5 < C_{obs} < 36$ g/L) were obtained (Fig. 4), indicating an acceptable calibration (Kerrou *et al.*, 2010). Furthermore, the main hydraulic features of the aquifer including the highest gradients in the Somâa aquifer and water table depression in the centre of the aquifer were reproduced.

The overall calibration of the model was considered sufficient to use the model for predicting the uncertainty affecting head and salt concentration distributions within the Korba aquifer.

3.3 Monte Carlo simulations and grid computing

A standard Monte Carlo method was used. For each realization, the numerical model was run (in transient regime for 44 years), changing only the discharge rates. The resulting outputs are post-processed to obtain ensemble statistics and probability maps of

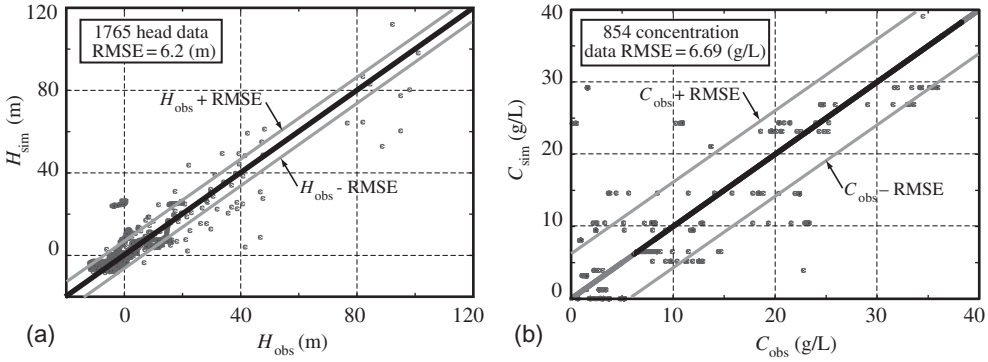

Fig. 4 Scatter plot showing the fits between the observed and calculated concentrations: (a) heads (m) and (b) salt concentrations (g/L). In both cases, observed values ±RMSE (root mean squared error) are also shown.

heads and concentrations. Each single simulation required more than 14 hours of computing time (on a Linux AMD Opteron 64-bit machine). To circumvent the large amount of computing time required to complete a sufficient number of simulations, the numerical simulations were run concurrently on the Grid infrastructure developed by the European EGEE project (http://www.eu-egee.org). The EGEE platform consists of over than 68 000 CPUs in addition to about 20 Petabytes of storage. The EGEE Grid includes more than 120 partners in 48 countries organized in 13 geographically dispersed collaboration groups (virtual organizations), focused on their specific research areas. A particularly interesting aspect offered by this emerging technology is that non-European partners, e.g. Tunisian academic researchers and water managers, can run their groundwater simulations via a web portal on the same Grid platform via the EGEE companion project EUMEDGRID (http://www.eumedgrid.org). Note that Monte Carlo simulations of density-dependent flow and transport were carried out using both CODESA3D (Gambolati *et al.*, 1999) and GroundWater (Cornaton, 2007) simulators for comparison and validation.

4 RESULTS

4.1 Discharge rates

The ensemble average of the 100 pumping rates realizations was similar to the regression estimation of Kerrou *et al.* (2010). Figure 5 shows two example realizations. In 1985 and 2004, the total estimated exploitation volumes are 50 and 47 hm^3/year, respectively. The 100 simulated pumping rates maps all have the same total abstraction volume, as the average simulated residual is null. The magnitude of absolute residuals, which is randomly distributed for each simulation in all wells, is 31.25 and 29.3 hm^3 in 1985 and 2004, respectively, corresponding to 62.5% of the total abstraction volume.

At each point, the groundwater abstraction can be highly variable through the 100 simulations, as shown for two candidate wells (240 and 361) in Fig. 5(c) and 5(d). The median value of the ratio Q_{max}/Q_{min} is 6.5 and depends on the well location. The average pumping rate on a single grid cell is 31.5×10^3 m^3/year in 2004. Figure 5(e) shows the typical time evolution of the pumping rates from 1960 to 2004, which was used for all wells.

4.2 Grid computing

The simulations were executed on the EGEE infrastructure. Each simulation was launched separately with the help of Unix shell scripts which execute different tasks (e.g. naming, decompressing, copying files) and a JDL (Job Description Language) file that described all input and output files (of the simulator) and the requirements for the job, launched the job (using gLite commands) on the grid, monitored the job, and transferred back the results. Three technical difficulties were encountered during that procedure. First, the middleware was not stable. It was necessary to adapt the shell scripts regularly. Second, a significant number of jobs (between 20 and 30%) were not executed because of reliability problems in the infrastructure. Third, transferring the files was time consuming, but this could have been optimized by running the post-processing on the Grid as well, instead of doing it locally after having transferred back all the files. This experience showed that it is still more

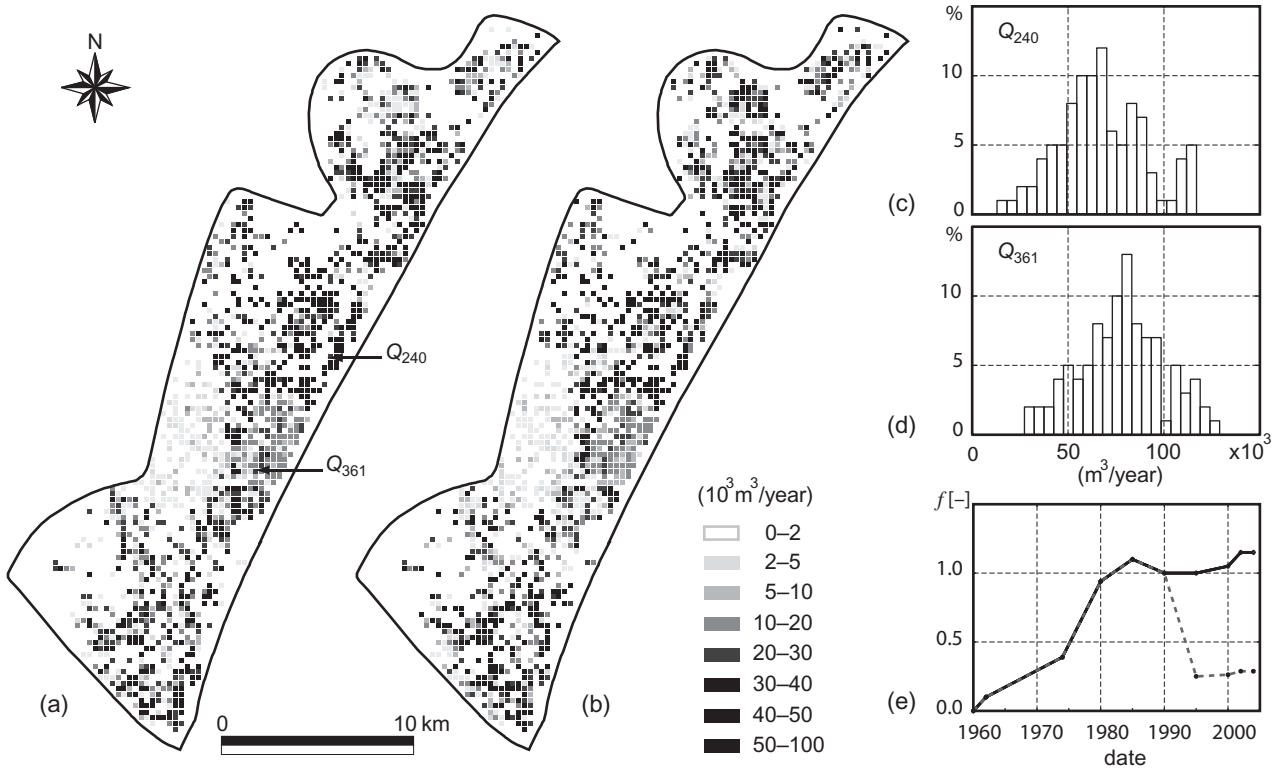

Fig. 5 (a) and (b) Example maps of the pumping rates (Q_c 1996). (c) and (d) Histograms of pumping rates for wells 240 and 361. (e) Time-dependent evolution functions for both wells (Q_{240}: —— and Q_{361}: - - - -) with 1996 volumes as reference.

difficult to run Monte Carlo simulations on a Grid infrastructure than on a local cluster, but it could be done successfully.

4.3 Monte Carlo simulations

First of all, the ensemble average head and concentration distributions (Fig. 6(a) and (b)) are in agreement with the conceptual model of the aquifer as well as the observed heads in 2004 (compare Fig. 1 and Fig. 6(a)). Ensemble average maps show very well the large depression in the central zone of the aquifer and the consequent seawater intrusion.

However, it is important to note that the map of ensemble average heads over 100 simulations is different from that of heads calculated using the average pumping. The same occurs for concentrations. This is normal and due to the nonlinearity of the flow and transport equations as was shown, for example, by Delhomme (1979). It is worth noting that predictions of ensemble averages of head and concentration distributions are more robust, compared to the solutions resulting from use of average pumping. Note that model parameters were not calibrated for each simulation of the pumping rates.

In addition to ensemble averages, the probability distribution functions of heads and concentrations at any point, and the probability maps for exceeding a certain concentration or head threshold, were calculated. Figure 7 shows the histograms of heads and concentrations in two arbitrary wells (361 and 240). The histograms reflect the effects of uncertain pumping rates on heads and concentrations and also show that small concentrations are more uncertain (compare Fig. 7(c) and (d)). The same figure also shows that higher pumping rates (on average) led to higher uncertainty (compare Fig. 5(c) and (d) and Fig. 7(c) and (d)). Figure 8 shows the probability maps of exceeding a relative concentration of 0.1 (Fig. 8(b)) and of the water table falling below the mean sea level (Fig. 8(a)). These maps are graphically not very different from the maps one could build based on a direct geostatistical interpolation of heads or concentrations. Making such an analysis would allow one to map the heads and concentrations and evaluate the uncertainty related to the lack of head or concentration data. However, making such maps may not be easy because

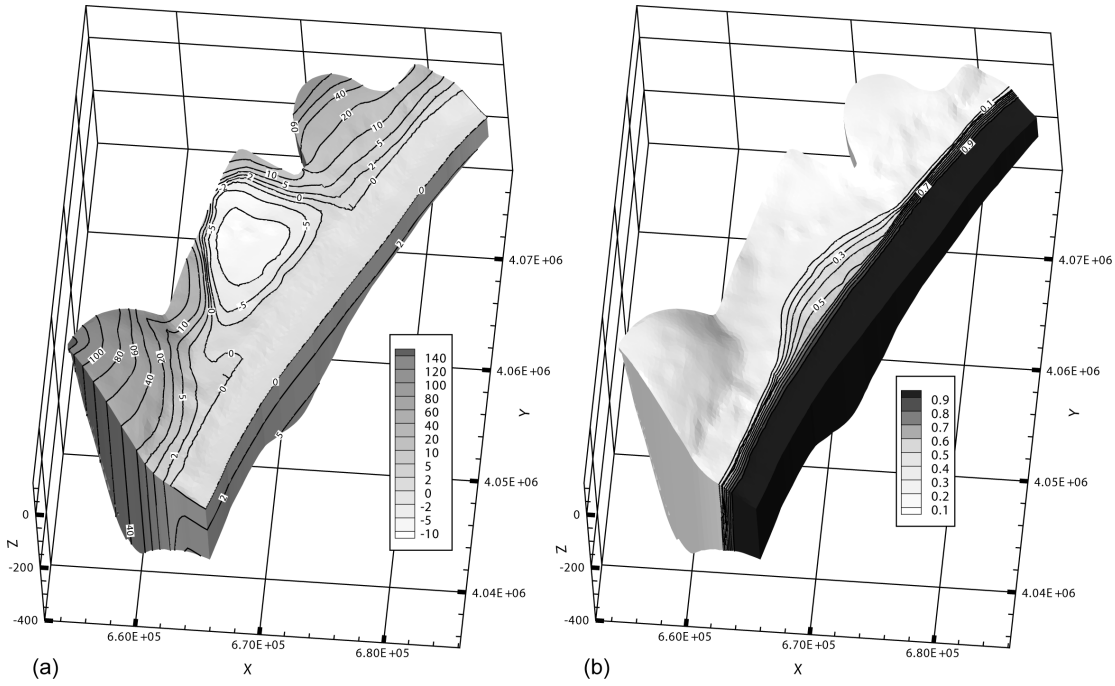

Fig. 6 Ensemble average maps for the 100 realizations: (a) head H (m); and (b) relative concentration C (-).

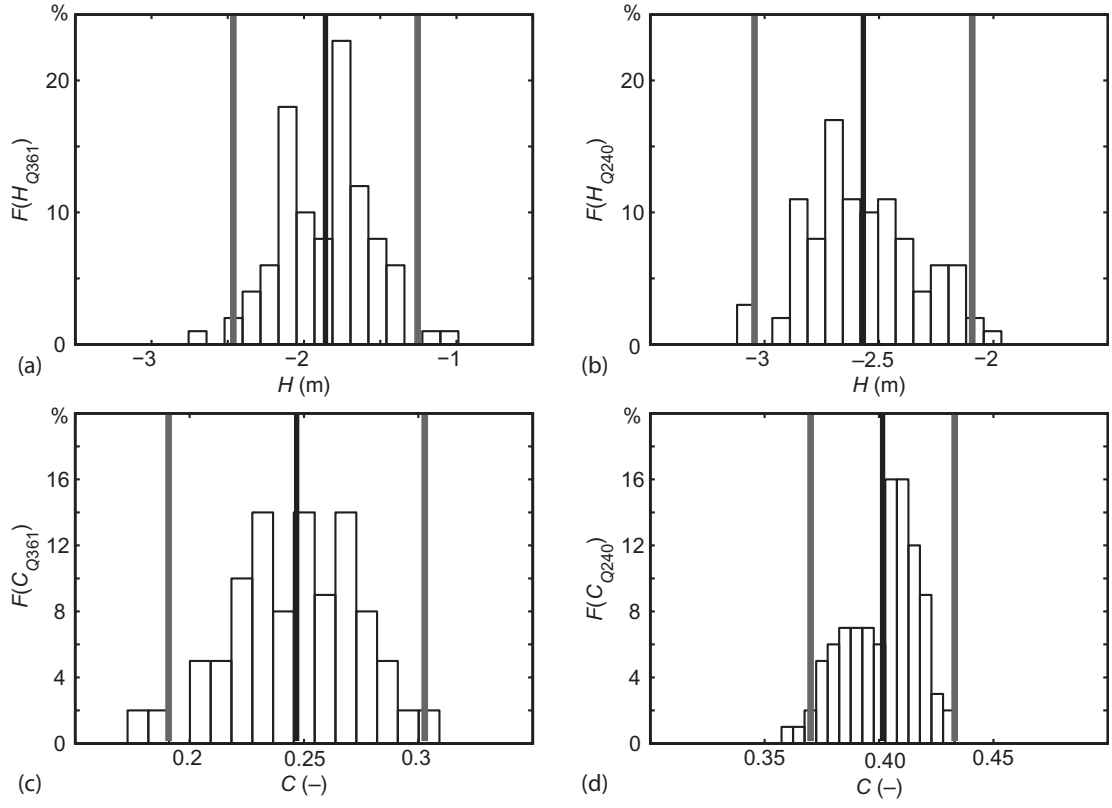

Fig. 7 Histograms of: (a) and (b) head H (m), and (c) and (d) relative concentration C (-) in wells Q_{361} and Q_{240}, respectively. Ensemble average (——) and ensemble average ±2 ensemble standard deviations (grey lines) are also shown.

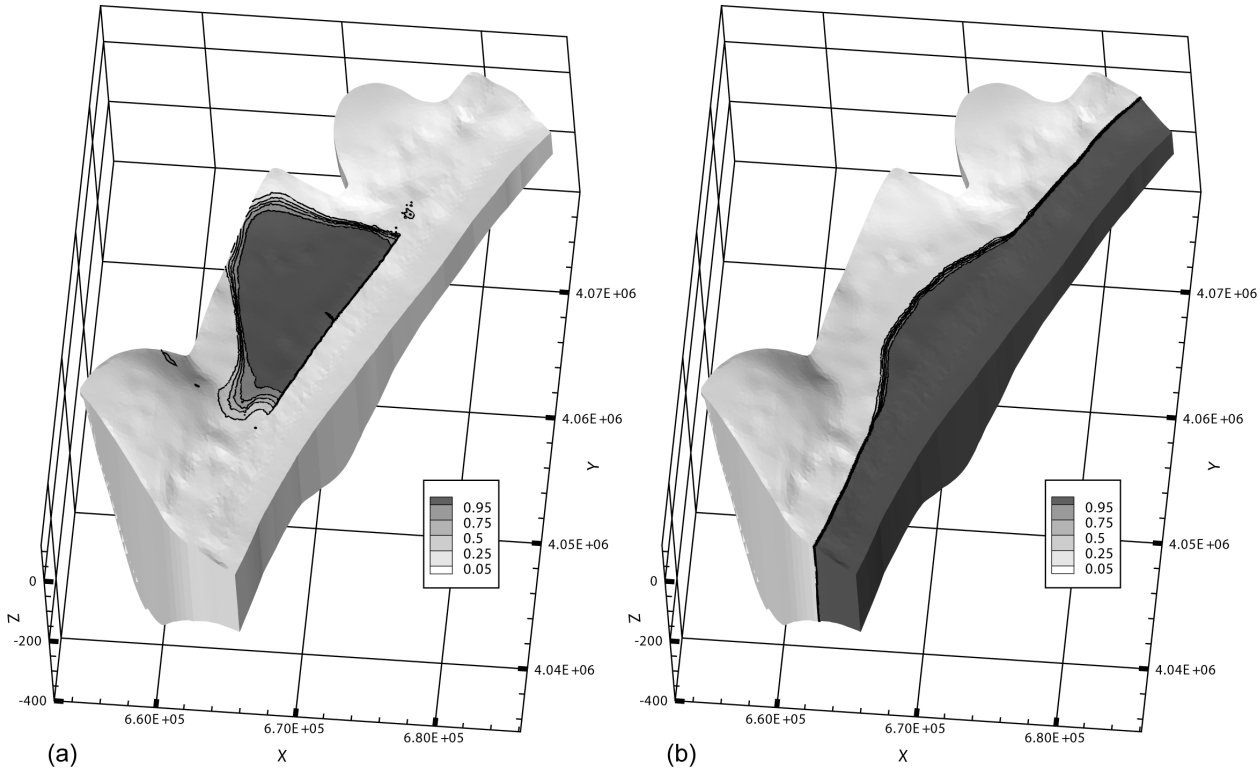

Fig. 8 Probability map for a point (a) to be under the mean sea level and (b) to exceed the 0.1 relative salt concentrations. Both maps show 0.95, 0.75, 0.5, 0.25 and 0.05 isoprobability contours.

neither the heads nor the concentrations are stationary in space and time. The geostatistical analysis would then need to be rather sophisticated; furthermore, such a study would not account for the physics of the processes. The maps shown in Figs 6 and 8 have a different meaning. They represent the uncertainty in heads and concentrations resulting from an evaluation of the uncertainty in the discharge rates. They are interesting because they all respect the basic physics used in the 3-D density-dependent flow and solute transport model. Because other uncertainties were not accounted for, they also represent a lower bound of the uncertainty.

Analysing the results more precisely, one can extract the regions where the probabilities are intermediate. These correspond to the maximum uncertainty. For example, in 2004 the area delimited by the 0.05–0.95 isoprobability contours of exceeding the 0.1 relative concentration (U_C) covers a fraction of about 4% of the total onshore area of the aquifer. This means that the spatial distribution of uncertainty in the exploitation rates leads to a rather small uncertain area in which seawater intrusion may or may not be encountered.

Another way of looking at the problem is to estimate the area in which it is not known precisely whether the groundwater levels are below sea level. For that purpose, one can compute the area delimited by the 0.05–0.95 probability contours of being below the mean sea level (U_H). It was found that this is about 8% of the area of the aquifer. Geographically, Fig. 8(a) and 8(b) shows that the large uncertainties in heads and concentrations are located around the piezometric depression in the central part of the aquifer and at the advancing seawater front.

Analysis of the temporal evolution of the uncertainty indicators (Fig. 9) reveals a different behaviour for heads and concentrations (U_H and U_C). Initially, there is no uncertainty, because all realizations start from the same initial state (i.e. no pumping). Then the uncertainty in heads rises rapidly with increasing discharge; it does not decrease, even when the discharge decreases. The uncertainty in concentrations rises regularly too, but at a smaller rate. This is explained by two factors. On one hand, the flow equation reacts faster than the transport equation; on the other, the two processes do not affect the same domain: seawater intrusion occurs only on a strip along the coast, while the piezometric map reacts everywhere in the domain.

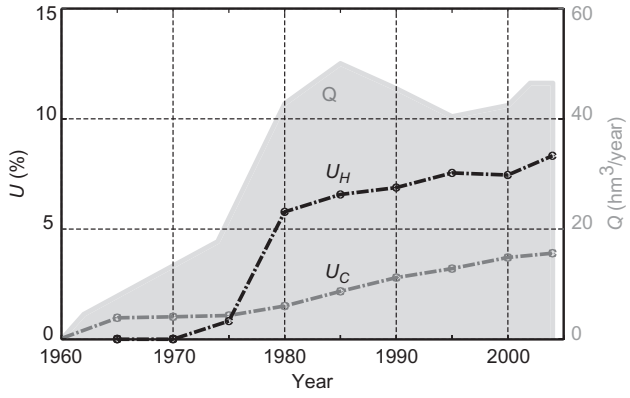

Fig. 9 Time evolution of the uncertainty: Q (grey polygon) represents the total estimated exploitation volume (hm^3), U_H is the ratio (%) between the uncertain area with respect to the probability of falling below sea level and the onshore aquifer area; and U_C is the ratio (%) between the uncertain area with respect to the probability of exceeding 0.1 relative concentration and the onshore aquifer area.

The same normalization constant (area of the aquifer) for both processes is arbitrary was used.

5 DISCUSSION AND CONCLUSIONS

The aims of this work were to investigate how to evaluate the uncertainty associated with the spatial distribution of pumping rates in the Korba aquifer and to test whether grid computing could be used for the Monte Carlo analysis. For that purpose, a geostatistical analysis of the spatial distribution of pumping rates coupled with Monte Carlo simulations were deployed on the distributed computing infrastructure provided by the EGEE Grid platform.

Surprisingly, it was found that the uncertainties in model predictions were small. The hydraulic head uncertainties were larger than those in salt concentration distributions. There are several interpretations for such a moderate level of predicted uncertainty. First, all the other aquifer parameters were kept constant to separate the effect of the uncertainty associated with the spatial distribution of the pumping rates from that associated with other model parameters. Indeed, it is believed that the uncertainty in hydraulic head and salt concentration distributions would be greater and would behave differently if multiple uncertain parameters were considered (e.g. uncertain pumping rates and uncertain hydraulic conductivity). Furthermore, the variogram model used to simulate the correction terms, and therefore the variability between the simulations, has a small range compared to the extent of the model. As a consequence, in spite of the fact that two neighbouring wells might have very different pumping rates in the same simulation, this would be compensated by the redistribution of the pumping rates between different simulations. However, even if the area delimited by the isolines 0.05 and 0.95 of the probability of exceeding the 0.1 relative salt concentrations is small with respect to the extent of the aquifer, it still covers more than 1300 ha and represents high potential losses in agricultural production resulting in a high socio-economic impact on the local population. Furthermore, this area is expected to continue to increase due to the time-shift between the evolution of the uncertain area and the evolution of the pumping rates (Fig. 9).

In terms of grid computing, the experience showed that it was more difficult to handle Monte Carlo simulations on the EGEE infrastructure than on a regular cluster. This was mainly due to the fact that the technology was still in development during our tests and that we faced instability problems with both the middleware and the infrastructure. However, the grid could be used remotely to launch simulations from different locations in Europe (Sardinia and Switzerland). With the rapid advances in Grid technology, it is expected that the reliability and stability issues will soon be overcome and that the technology will rapidly become completely transparent for the user. It is clear that this will provide a formidable opportunity for countries or researchers having limited access to local computing resources.

Acknowledgements This work was funded by the Swiss National Science Foundation (grants 207020-110017 and PP002-106557) and the Sardinian Regional Authority HYDROMED (L.R. 19/96). The authors thank Monique Petitdidier and Roberto Barbera for their support with the EGEE Grid technology. The authors are also grateful to Aldo Fiori for his constructive review.

REFERENCES

Abarca, E. (2006) *Seawater Intrusion in Complex Geological Environments*. Barcelona: Technical University of Catalonia.

Al-Bitar, A. & Ababou, R. (2005) Random field approach to seawater intrusion in heterogeneous coastal aquifers: unconditional simulations and statistical analysis. In: *Geostatistics for Environmental Applications* (P. Renard, H. Demougeot-Renard & R. Froidevaux, eds). Berlin: Springer.

Bear, J., Cheng, A. H. D., Sorek, S., Ouazar, D. & Herrera, I. (1999) *Seawater Intrusion in Coastal Aquifers – Concepts,*

Methods and Practices. Dordrecht: Kluwer Academic Publishers.

Carrera, J. (1993) An overview of uncertainties in modeling groundwater solute transport. *J. Contam. Hydrol.* **13**(1–4), 23–48.

Cheng, A. H. D. & Ouazar, D. (2003) *Coastal Aquifer Management: Monitoring, Modeling, and Case Studies*. Boca Raton, FL: Lewis.

Cornaton, F. (2007) *GroundWater: A 3-D Ground Water Flow and Transport Finite Element Simulator.* Reference Manual, http://www1.unine.ch/chyn/php/softwares.php.

Custodio, E. (2002) Aquifer overexploitation: what does it mean? *Hydrogeol. J.* **10**(2), 254–277.

Dagan, G. & Zeitoun, D. G. (1998) Seawater–freshwater interface in a stratified aquifer of random permeability distribution. *J. Contam. Hydrol.* **29**(3), 185–203.

Delhomme, J. P. (1979) Spatial variability and uncertainty in groundwater-flow parameters – geostatistical approach. *Water Resour. Res.* **15**(2), 269–280.

Diersch, H.-J. G. & Kolditz, O. (2002) Variable-density flow and transport in porous media: approaches and challenges. *Adv. Water Resour.* **25**, 899–944.

Doherty, J. (1998) *PEST – Model Independent Parameter Estimation*. Brisbane: Watermark Numerical Computing.

Ennabli, M. (1980) Etude hydrogéologique des aquifères du nord-est de la Tunisie pour une gestion intégrée des ressources en eau. Thèse de Doctorat d'État, Université de Nice, France.

Foster, I. & Kesselman, C. (1998) Computational Grids. In: *The Grid: Blueprint for a New Computing Infrastructure* (I. Foster & C. Kesselman, eds). San Francisco: Morgan Kaufmann, Inc.

Gambolati, G., Putti, M. & Paniconi, C. (1999) Three-dimensional model of coupled density-dependent flow and miscible transport in groundwater. In: *Seawater Intrusion in Coastal Aquifers: Concepts, Methods, and Practices* (J. Bear *et al.* eds), 315–362. Dordrecht: Kluwer Academic Publishers.

Kerrou, J., Renard, P. & Tarhouni, J. (2010) Status of the Korba groundwater resources (Tunisia): observations and three-dimensional modelling of seawater intrusion. *Hydrogeol. J.* **18**(5) 1173–1190. doi:10.1007/s10040-010-0573-5.

Khlaifi, I. (1998) Contribution à l'étude de l'intrusion marine par un modèle de transport tridimensionnel: interfaçage avec des systèmes d'information géographique. Thèse de master, Institut National Agronomique de Tunisie.

Konikow, L. F. & Kendy, E. (2005) Groundwater depletion: a global problem. *Hydrogeol. J.* **13**(1), 317–320.

Kouzana, L., Ben Mammou, A. & Sfar Felfoul, M. (2009) Seawater intrusion and associated processes: case of the Korba aquifer (Cap-Bon, Tunisia). *C. R. Geosci*. **341**(1), 21–35.

Matheron, G. (1973) The intrinsic random functions and their applications. *Adv. Appl. Probability.* **5**, 439–468.

Milnes, E. & Renard, P. (2004) The problem of salt recycling and seawater intrusion in coastal irrigated plains: an example from the Kiti aquifer (Southern Cyprus). *J. Hydrol.* **288**(3–4), 327–343.

Naji, A., Cheng, A. H. D. & Ouazar, D. (1998) Analytical stochastic solutions of saltwater/freshwater interface in coastal aquifers. *Stochast. Hydrol. Hydraul.* **12**(6), 413–430.

Oueslati, A. (1994) Les côtes de la Tunisie. Recherche sur leur évolution au Quaternaire. Tunis: Imprimerie officielle de la Republique Tunisienne.

Paniconi, C., Khlaifi, I., Lecca, G., Giacomelli, A. & Tarhouni, J. (2001) Modeling and analysis of seawater intrusion in the coastal aquifer of eastern Cap-Bon, Tunisia. *Trans. Porous Media.* **43**(1), 3–28.

Slama, F., Milnes, E. & Bouhlila, R. (2008) Calibrating unsaturated model parameters using electrical resistivity tomography imaging. In: *Calibration and Reliability in Groundwater Modelling: Credibility of Modelling* (J. C. Refsgaard, K. Kovar, E. Haarder & E. Nygaard, eds), 148–153. Wallingford: IAHS Press, IAHS Publ. 320.

Sorek, S. & Pinder, G. F. (1999) Survey of computer codes and case histories. In: *Seawater Intrusion in Coastal Aquifers: Concepts, Methods, and Practices* (J. Bear *et al.*, eds), 399–461. Dordrecht: Kluwer Academic Publishers.

Steenhuis, T. S. & Vandermolen, W. H. (1986) The Thornthwaite-Mather procedure as a simple engineering method to predict recharge. *J. Hydrol.* **84**(3–4), 221–229.

Tarhouni, J., Jemai, S., Walraevens, K. & Rekaya, M. (1996) Caracterisation de l'aquifere côtier de Korba au Cap Bon (Tunisie). *Progress Report 95-96 for AVI-73 EC Project.*

Tompson, A. F. B., Ababou, R. & Gelhar, L. W. (1989) Implementation of the 3-dimensional turning bands random field generator. *Water Resour. Res.* **25**(10), 2227-2243.

United Nations Foundation (2008) *UN Atlas of the Oceans*. http://www.oceansatlas.org/.